NANO LETTERS

2008
Vol. 8, No. 2
511−515

Height Independent Compressive Modulus of Vertically Aligned Carbon Nanotube Arrays

Tao Tong,[†] Yang Zhao,[‡] Lance Delzeit,[§] Ali Kashani,[‡] M. Meyyappan,[§] and Arun Majumdar*,[†,||]

Department of Mechanical Engineering, University of California, Berkeley, California 94720, Atlas Scientific Inc., 1367 Camino Robles Way, San Jose, California 95120, Center for Nanotechnology, NASA Ames Research Center, Moffett Field, California 94035, and Materials Sciences Division, Lawrence Berkeley National Laboratory, Berkeley, California 94720

Received October 20, 2007; Revised Manuscript Received December 7, 2007

ABSTRACT

The compressive modulus of dense vertically aligned multiwalled carbon nanotube (CNT) arrays synthesized by chemical vapor deposition was investigated using an optically probed precision-loading platform. For CNT arrays with heights ranging from 15 to 500 μm, the moduli were measured to be about 0.25 MPa and were found to be independent of array height. A continuum mechanics model based on multimode buckling guided by the wavy features of CNT arrays is derived and explains well the measured compressive properties. The measured compressive modulus of the CNT arrays also satisfies the "Dahlquist tack criterion" for pressure sensitive adhesives, which was previously observed for these vertically aligned CNT arrays (Zhao, Y., et al. *J. Vac. Sci. Technol., B* 2006, *24*, 331−335).

While major research interests in the mechanical properties of carbon nanotubes lie in the characterization of individual carbon nanotubes (CNTs)[1,2] or composite materials with dispersed CNTs,[3−6] mechanical properties of CNTs in the form of a dense vertically aligned array have been relatively scarce in the literature.[7,8] Cao et al.[7] reported a super-compressible characteristic of vertically aligned CNT arrays that are ∼1 mm long and observed wavelike folding of the CNT arrays during compression due to multimode buckling. Deck et al.[8] recently studied the tensile and compressive behavior of CNT mats. However, in both studies the length dependence of the elastic moduli was not discussed specifically. The goal of this paper is to investigate the compressive properties of CNT arrays and explore its array height dependence. We found that the compressive moduli are almost independent of array height for heights spanning over 1 order of magnitude range, and identify the underlying reason.

Dense vertically aligned CNT arrays were synthesized on rigid substrates by chemical vapor deposition (CVD). The substrates used in this work were silicon (Si) wafers with thickness of 500 μm. Before deposition, the Si substrates were ion-beam sputtered with a thin layer of iron (Fe) as catalyst on top of an aluminum (Al) adhesion layer. The feedstock gas was ethylene, and the substrate was locally heated to ∼750 °C when growth of CNTs was initiated. Details about carbon nanotube growth can be found elsewhere.[9,10] The as-grown CNT arrays had tube diameters 20−30 nm with an aerial density $\sim 10^{10}$ tubes/cm^2. The array heights (length of CNTs) were controlled by growth time and ranged from ∼10 μm to more than 500 μm. Figure 1 shows a typical side view of an as-grown CVD CNT array with array height ∼50 μm. The CNTs are inherently wavy along their lengths.

A home-built optically probed loading platform using Michelson interferometry and a reflective cantilever tip was used to measure the displacement and force (Figure 2a). The loading stage consists of two parts, namely: (i) a glass cantilever beam on one side, and (ii) a piezoelectric kicking stage on the other side providing the actuation. The glass cantilever acts as a displacement and force sensor. The cantilever displacement is monitored by a laser beam reflected from the tip. The spring constant of the cantilever can be determined from measuring the fundamental mode resonant frequency. Knowing the displacement and spring constant allows us to determine the force. On the other side, the loading stage is actuated by a piezoelectric element (PZT) through continuous kicking actions of the PZT. The PZT

* Corresponding author. E-mail: majumdar@me.berkeley.edu.
[†] University of California.
[‡] Atlas Scientific Inc.
[§] NASA Ames Research Center.
[||] Lawrence Berkeley National Laboratory.

10.1021/nl072709a CCC: $40.75
Published on Web 01/12/2008

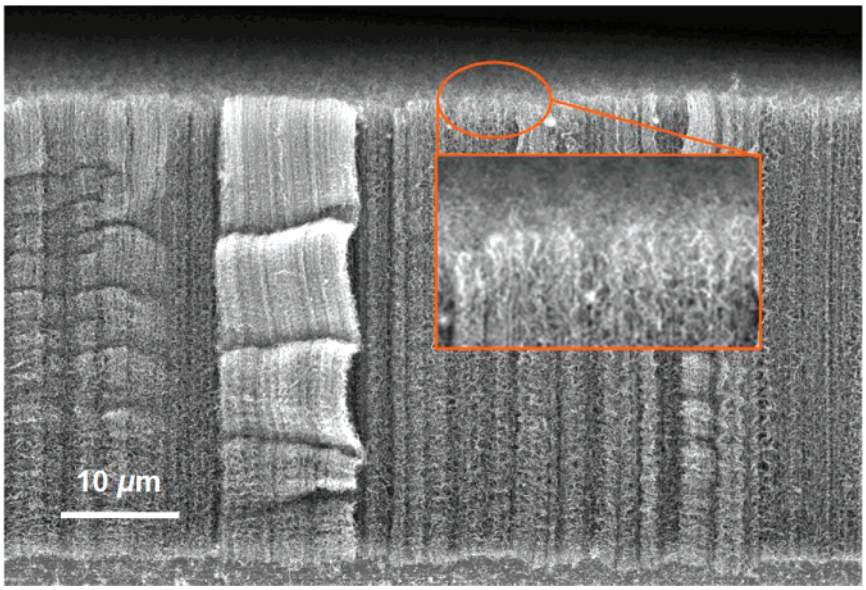

Figure 1. SEM side view of a vertically aligned multiwalled CNT array. These CNTs are shown to have intrinsic wavy features. The inset shows the unevenness at the free top surface of the CNT array.

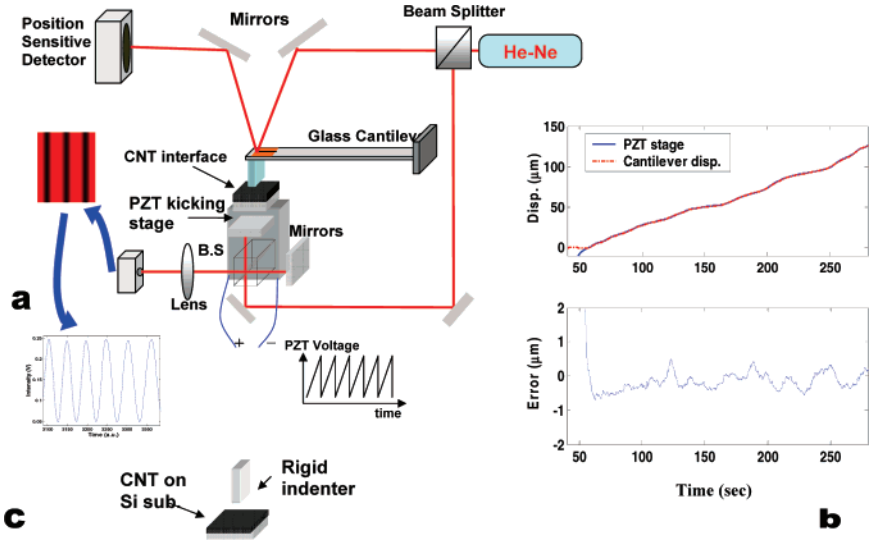

Figure 2. (a) Schematics of the optically probed precision-loading platform for indentation characterization of CNT arrays. (b) Calibration curves of the loading platform using a rigid interconnect between the cantilever tip and the PZT stage: The upper figure records the displacements from both the PSD and the Michelson interferometer as the PZT stage moves toward one direction; the lower graph shows the difference between the two position recordings throughout the loading process, and the error is within ± 0.5 μm. (c) Experimental schematic showing the compression test to characterize the compressive properties of CNT arrays.

kicking stage follows the design of Silveira and Marohn,[11] and a detailed description can be found in their paper. In our experiments, the PZT stage was driven by a sawtooth voltage signal at a frequency of 666 Hz and maximum amplitude of 10 V (peak-to-peak). The relative high frequency is needed to achieve a smooth motion. The actual displacement of the PZT stage is monitored by a Michelson interferometer mounted on the stage. A typical time trace of the optical intensity signal (128 Hz sampling rate with a moving speed ~3 fringes per second or ~1 μm/s) is shown in the lower-left inset of Figure 2a. We applied a sinusoidal phase interpolation algorithm to the oscillating intensity signal. With this interpolation, a resolution of ~10 s of nanometer can be achieved.[12] However, the overall displacement resolution of the current platform is limited by the cantilever tip at a lower resolution ~0.5 μm. The interferometer and the optical reflecting cantilever were placed inside a box to isolate the optical setup from disturbances from the environment. The loading platform can operate in tensile or compressive mode by changing the direction of actuation. Therefore, the same setup was also applied to the measurement of the adhesive (tensile) properties of the CNT arrays.

Figure 2c shows the schematic for compressive tests. A rigid strut (quartz, end cross-sectional dimension of 0.5 mm × 2 mm), which is attached to the cantilever tip, is pressed into the CNT array, whose substrate is glued to the moving part of the PZT kicking stage in the direction perpendicular to the array surface. The force-displacement relation is

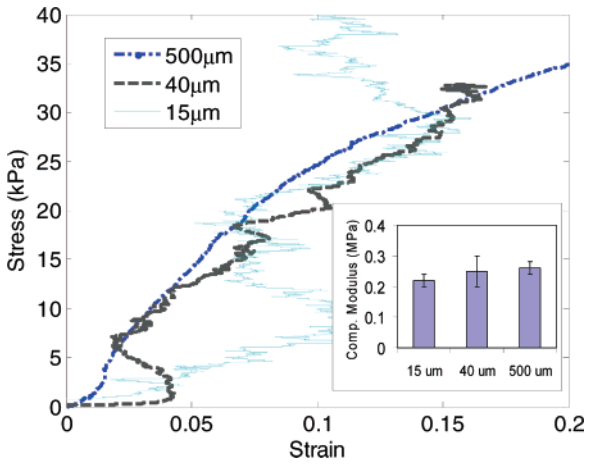

Figure 3. Representative stress−strain curves from the compression tests of 15, 40, and 500 μm tall CNT arrays with an apparent contact area of the strut 0.5 mm × 2 mm. The inset shows the effective compressive moduli of the CNT arrays evaluated at a strain of 10%. The error bars indicate the standard deviations from three repeated tests for each sample.

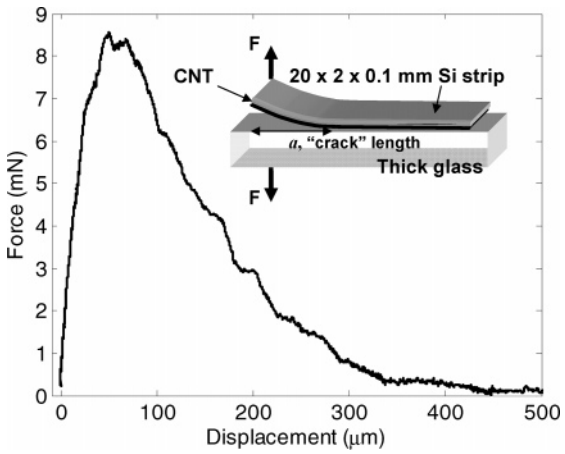

Figure 4. Interface work of adhesion measured by the "peel-test". Multiwalled carbon nanotubes were first grown on a slender strip of Si substrate. The CNT array was then pressed and adhered onto a rigid glass substrate and pulled apart by the same loading platform. As a quasi-static peeling process, the interface work of adhesion is evaluated by taking the area under the force-displacement curve divided by the apparent contact area of the strip to the glass surface.

recorded during the compression. With the loading curve, the compressive modulus of the CNT array can be calculated. Note that the maximum cantilever tip displacement is on the order of 100 μm. With a cantilever length of 60 mm, the maximum angular rotation of the tip and the strut is estimated ~0.1°.

The stress−strain curves under compressive loading of 15, 40, and 500 μm tall CNT arrays are shown in Figure 3. The stress−strain curves are converted from the directly measured force and displacement relations by

$$E_{\text{comp}} = \left(\frac{F}{A}\right) / \left(\frac{\Delta L}{L}\right) \quad (1)$$

where A is the apparent contact area. The fluctuation in the stress−strain curves, especially for short arrays, is because these curves represent real time traces of the loading processes and thus reflect possibly uneven contact as well as the measurement resolution in displacement ~0.5 μm. From the measurements during CNT array compression, we calculate the E_{comp} (shown in the inset of Figure 3) to be 0.22 ± 0.02 MPa for the 15 μm tall CNT array, 0.25 ± 0.05 MPa for the 40 μm tall CNT array, and 0.25 ± 0.02 MPa for the 500 μm tall CNT array. The error bars represent the standard deviation for three repeated tests for each sample. Despite the large difference in array height, the elastic moduli are found to be surprisingly close.

It was previously shown that the CVD grown multiwalled carbon nanotube arrays could show dry adhesive properties due to van der Waals interactions with proper preloading,[13] similar to pressure sensitive adhesives.[14] As experimentally studied by Dahlquist[15] earlier on various kinds of tacky adhesives, it was empirically concluded that all the adhesives need to have modulus less than 0.3 MPa in order to show tack.[14,15] Therefore, the relative softness of the CNT arrays may have been one of the key reasons to the observed dry adhesive properties in our previous study.[13] A similar structural feature was also found in gecko setal arrays.[16] While the Dahlquist criterion may provide a necessary condition for tack, the dry adhesion was also shown to depend on the array height: CNT arrays with height less than 50 μm showed adhesion and typically the shorter the better.[13] It is possible that the elastic energy stored in the array during preloading may adversely affect the adhesion interface by releasing the energy into the interface and thereby peeling it apart. The typical interface work of adhesion was characterized by a "peel-test"[17,18] shown in Figure 4 and was found to be around 36 mJ/m^2, which is in the typical range of van der Waals interfaces. Considering a 30 μm tall CNT array with an effective modulus of 0.25 MPa, it takes only about 10% of strain to store a similar amount of elastic energy in the CNT array as the interface work of adhesion. Therefore, it is likely that as the array gets taller it is easier to store larger amount of elastic energy in the array so that the adhesion interface becomes unstable.

Note, however, that our measured values of elastic modulus are significantly smaller than those reported by Cao et al.,[7] of ~50 MPa for an 860 μm tall CNT array and Deck et al.[8] of 818 MPa for a CNT array taller than 1 mm. The big difference could be due to multiple reasons involving growth-dependent structure of CNT arrays as well as the loading scheme. In their work,[7,8] they used vapor-phase floating ferrocene as the catalyst. Multiwalled CNTs grown by vapor-phase floating ferrocene catalysts can easily reach millimeters in length but were also shown to have less crystallinity, more catalyst residuals, and even multiple junctions along tubes enhancing coupling among neighboring tubes comparing with predeposited catalytic growth of CNTs[19−22] and therefore usually stiffer. The CNTs in our work showed less cross-tube coupling because sharp-edged dents in the arrays were left after indentation. Yap et al.[23] recently characterized the behavior of an individual multiwalled CNT under compressive loading by an atomic force microscopy tip. From their force-displacement relation of a

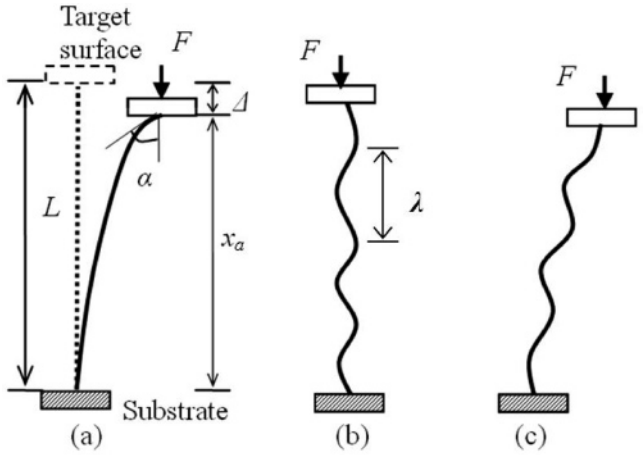

Figure 5. Structural model of the buckling of a carbon nanotube with independent tube assumption: (a) fundamental mode buckling; (b) higher-mode buckling; (c) higher-mode buckling with bending.

6.6 μm long CNT (30 nm tube diameter and aspect ratio of 220), the compressive modulus would be ~60 MPa assuming an array of tube density of 10^{10} cm^{-2} in the prebuckling range and ~6 MPa in the range after buckling (for strain <25%). It seems that our loading processes did not have the prebuckling regime of pure compression possibly due to: (i) uneven length distribution of the CNTs and (ii) the quartz-strut might not be perfectly parallel to the CNT top surface. As a result, the CNTs did not buckle at the same time, but sequentially.

To understand the mechanism that produces the observed compressive modulus, we first consider a fundamental mode buckling theory. We neglect the surface entanglement and the interactions of the neighboring nanotubes. As shown in Figure 5a, each nanotube is modeled as an elastic beam of length L with Young's modulus E and area moment of inertia I. The beam is subject to a compressive load, F, which is applied downward on the tip. When F exceeds the critical load $F_{cr} = \pi^2 EI/(4L^2)$, the nanotube buckles (fundamental mode considering the clamp-hinge boundary condition) causing the tip to deflect by an angle α. Following from the equations of motion for an elastic beam, the normalized vertical displacement or strain of the tip can be expressed as[24]

$$\frac{\Delta}{L} = 2 - \frac{4}{\pi} E(p) \sqrt{\frac{F_{cr}}{F}} \tag{2}$$

where $p \equiv \sin(\alpha/2)$ and the solution is

$$K(p) = \frac{\pi}{2} \sqrt{\frac{F}{F_{cr}}} \tag{3}$$

Here, the functions $K(\bullet)$ and $E(\bullet)$ are the complete elliptic integrals of the first and second kind, respectively. For small α, $E(p) \approx (\pi/2)(1 - p^2/4)$ and $K(p) \approx (\pi/2)(1 + p^2/4)$.[25] Substituting these expressions into the above equations and solving for the normalized load, one obtains the force-displacement relation approximated for small displacement

$$\frac{F}{F_{cr}} = 16\left(4 - \frac{\Delta}{L}\right)^{-2} \tag{4}$$

Taking the derivative of force (F) with respect to displacement (Δ), one obtains the compressive modulus approximated for small strain (Δ/L)

$$E_{comp} = \frac{dF}{d\Delta}\frac{L}{A} \approx \frac{F_{cr}}{2A_{CNT}} = \frac{\pi^2 EI}{8A_{CNT}L^2} \tag{5}$$

where A_{CNT} is the average area one tube occupies. An exact calculation without the small strain approximation gives about 20% larger E_{comp} than that from eq 5 at a strain of 10%.

Using a typical value $E = 1$ TPa for multiwalled CNT,[26] $I = \pi(D^4 - d^4)/64$, where the outer diameter $D = 25$ nm and inner diameter $d = 10$ nm, a tube density of 10^{10} cm^{-2}, and apparent contact area A of 0.5 mm $\times$ 2 mm, E_{comp} is calculated to be 10 kPa for the 15 μm tall array, which is about 22 times smaller than the measured 0.22 MPa, 1.4 kPa compared with the measured 0.25 MPa for the 40 μm tall array, and 9.2 Pa compared with the measured 0.25 MPa for the 500 μm tall array. Clearly, the model based on fundamental mode buckling does not explain our experimental results. Furthermore, the $E_{comp} \propto 1/L^2$ expressed in eq 5 is contradictory to the observed length-independent elastic moduli.

It is observed under scanning electron microscopy (SEM) that the CNTs are inherently wavy along the tube axis (see Figure 1). Under compressive loading, the buckling of the nanotube may be guided by the wavy nature of CNTs at a higher nth mode (Figure 5b) containing n waves from end to tip (the fundamental mode contains 1/4 wave with the assumed clamp-hinge boundary conditions). The wavy nature of CNTs under compressive loading was beautifully shown by Cao et al.[7] through cyclic loading.

Assume the nanotubes take an evenly distributed sinusoidal shape with a wavelength $\lambda = L/n$. Because a full wavelength can be regarded as four sections of the structure shown in Figure 5a being connected in series, it follows from eq 5 that the compressive modulus of the CNT in the nth mode buckling can be expressed as

$$E_{comp} = \frac{L}{4nA_{CNT}} \frac{\pi^2 EI}{8(\lambda/4)^3} = \frac{2\pi^2 EI}{A_{CNT}\lambda^2} \tag{6}$$

It follows that E_{comp} is independent of the array height, L, which agrees with our observations. To fit with our experimental measurements of E_{comp}, one can derive $\lambda \sim 12.9$ μm for the 15 μm tall array, $\lambda \sim 12.1$ μm for the 40 μm tall array, and $\lambda \sim 12.1$ μm for the 500 μm tall array. These values are close to those experimentally observed by us (see Figure 1) and those of Cao et al.[7] with $\lambda \sim 12$ μm for the 860 μm tall array. This matches the intuition that the buckling

waves are guided by the natural wrinkles of the CNTs and should be a structural characteristic of the CNT array regardless of the total length, as long as the overall morphology is the same.

Although strains larger than 20% were not explored experimentally in our current study due to the force constraint of the loading stage, the force-displacement curve of the 500 μm sample already showed softened E_{comp} at strain >10%, which indicates possibly mixed buckling and bending of the CNTs (Figure 5c).

In summary, we have used an optically probed precision-loading platform to study the compressive properties of the chemical vapor deposited dense vertically aligned multi-walled carbon nanotube arrays. From compressive tests to CNT arrays with tube lengths of 15, 40, and 500 μm, compressive moduli of the CNT arrays were found to be ~0.25 MPa due to sequential buckling and were almost independent of CNT array heights for strains up to 20%. A continuum mechanics model assuming noninteracting CNTs is derived indicating higher-mode buckling as the mechanism responsible for the compression of CNT arrays. The measured effective compressive moduli of the CNT arrays match the empirical Dahlquist criterion for tack and allow for the CNT arrays to show dry adhesive properties.

Acknowledgment. The authors thank Pramod Reddy for making the PZT kicking stage used in the study, and Dr. Richard E. Groff and Carmel S. Majidi for helpful discussions on the elastic model of CNTs. The financial support for this study was provided through NASA SBIR and ONR MURI programs.

References

(1) Yu, M. F.; Lourie, O.; Dyer, M. J.; Moloni, K.; Kelly, T. F.; Ruoff, R. S. *Science* **2000**, *287*, 637−640.
(2) Zhang, Y. Q.; Liu, G. R.; Wang, J. S. *Phys. Rev. B* **2004**, *70*, 205430.
(3) Thostenson, E. T.; Chou, T. W. *Carbon* **2004**, *42*, 3015−3018.
(4) Moniruzzaman, M.; Winey, K. I. *Macromolecules* **2006**, *39*, 5194−5205.
(5) Gibson, R. F.; Ayorinde, E. O.; Wen, Y. F. *Compos. Sci. Technol.* **2007**, *67*, 1−28.
(6) Ajayan, P. M.; Suhr, J.; Koratkar, N. *J. Mater. Sci.* **2006**, *41*, 7824−7829.
(7) Cao, A.; Dickrell, P. L.; Sawyer, W. G.; Ghasemi-Nejhad, M. N.; Ajayan, P. M. *Science* **2005**, *310*, 1307−1310.
(8) Deck, P. C.; Flowers, J.; McKee, G. S. B.; Vecchio, K. *J. Appl. Phys.* **2007**, *101*, 023512.
(9) Delzeit, L.; Nguyen, C. V.; Chen, B.; Stevens, R.; Cassell, A.; Han, J.; Meyyappan, M. *J. Phys. Chem. B* **2002**, *106*, 5629−5635.
(10) Delzeit, L.; Chen, B.; Cassell, A.; Stevens, R.; Nguyen, C.; Meyyappan, M. *Chem. Phys. Lett.* **2001**, *348*, 368−374.
(11) Silveira, W. R.; Marohn, J. A. *Rev. Sci. Instrum.* **2003**, *74*, 267−269.
(12) Vacuum wavelength of the He-Ne laser was used in the calculation of displacement. Cosine error resulting from the misalignment between the direction of motion and the normal axis of the plane mirror and other effects such as air refractivity, laser frequency, beam drifting, and thermal effect were not considered here because the overall precision of the loading platform was anyway limited by the reflecting cantilever and the signal of the PSD at ~0.5 μm.
(13) Zhao, Y.; Tong, T.; Delzeit, L.; Kashani, A.; Meyyappan, M.; Majumdar, A. *J. Vac. Sci. Technol., B* **2006**, *24*, 331−335.
(14) Pocius, A.V. *Adhesion and Adhesives Technology − An Introduction*; Hanser Gardner Publications: Cincinnati, OH, 1997.
(15) Dahlquist, C. A. Pressure-sensitive adhesives. In *Treatise on Adhesion and Adhesives*; Dekker: New York, 1969; Volume 2.
(16) Autumn, K.; Majidi, C.; Groff, R. E.; Dittmore, A.; Fearing, R. *J. Exp. Biol.* **2006**, *209*, 3558−3568.
(17) Dean, R. H.; Hutchinson, J. W. *Fracture Mechanics*; Wheeler, J. B., Ed.; American Society for Testing Materials: Philadelphia, PA, 1980; pp 383−405.
(18) Kim, J.; Kim, K. S.; Kim, Y. H. *J. Adhes. Sci. Technol.* **1989**, *3*, 175−187.
(19) Hart, A. J.; Slocum, A. H. *J. Phys. Chem. B* **2006**, *110*, 8250−8257.
(20) Deck, C. P.; Vecchio, K. S. *J. Phys. Chem. B* **2005**, *109*, 12353−12357.
(21) Lee, C. J.; Lyu, S. C.; Kim, H. W.; Park, C. Y.; Yang, C. W. *Chem. Phys. Lett.* **2002**, *359*, 109−114.
(22) Ting, J. M.; Li, T. P.; Chang, C. C. *Carbon* **2004**, *42*, 2997−3002.
(23) Yap, H. W.; Lakes, R. S.; Carpick, R. W. *Nano Lett.* **2007**, *7*, 1149−1154.
(24) Timoshenko, S. P.; Gere, J. M. *Theory of Elastic Stability*; McGraw-Hill: New York, 1961.
(25) Byrd, P. F.; Friedman, M. D. *Handbook of Elliptic Integrals for Engineers and Scientists*; Springer-Verlag: New York, 1971.
(26) Yakobson, B. I.; Avouris, P; Mechanical Properties of Carbon Nanotubes. In *Carbon Nanotubes: Synthesis, Structure, Properties and Applications*; Smalley, R. E., Dresselhaus, M. S., Dresselhaus, G., Avouris, P., Eds.; Springer: New York, 2001; Chapter 12.

NL072709A